

Earthquake Source Parameters and the Frequency Dependence of Attenuation at Coalinga, Mammoth Lakes, and the Santa Cruz Mountains, California

GRANT T. LINDLEY AND RALPH J. ARCHULETA

Department of Geological Sciences and Institute for Crustal Studies, University of California at Santa Barbara, Santa Barbara

Least squares best fits were calculated to the Fourier amplitude spectra of P and S waves of locally recorded earthquakes. Attenuation, amplification, and earthquake source parameters were calculated from parameters of the fits. Approximately 8200 spectra were fit at 39 sites at Coalinga, Mammoth Lakes, and the Santa Cruz Mountains, California. Typically, the spectra were fit from 2 to 45 Hz for P waves and 2 to 20 Hz for S waves. The source spectral falloff of P waves was limited to be no greater than $f^{-2.5}$ (f is frequency) by low attenuation sites in the Sierra Nevada. Attenuation was measured through t^* , the travel time divided by Q . Attenuation was considered to be frequency dependent according to $t^* = t_0^* f^{-\alpha}$, which is equivalent to $Q = Q_0 f^\alpha$. Negative values of α were found to minimize the sum of squared residuals at most of the sites studied. Attenuation and amplification varied from site to site systematically with site geology. Source parameters were determined for individual earthquakes by averaging fit parameters from between four and 18 spectra, depending on the earthquake. Seismic moments ranged from roughly 5×10^{12} to 10^{15} Nm at Coalinga and Mammoth Lakes. Moments ranged from 2×10^{11} to 3×10^{14} Nm in the Santa Cruz Mountains. When the fits were determined using negative values of α , the seismic moments trended approximately as f_c^{-3} (f_c is the corner frequency). For $\alpha = -0.5$, stress drops varied from roughly 0.2 to 50 MPa at Coalinga and Mammoth Lakes. Stress drops were lower in the Santa Cruz Mountains, ranging from approximately 0.05 to 8 MPa.

INTRODUCTION

Understanding the amplification and attenuation of seismic waves in the near surface is important in order to predict ground motion from earthquakes and in order to accurately determine source properties of earthquakes. In this paper the amplification and attenuation at a number of different sites are determined from the Fourier spectra of earthquakes. The amplification determined in this study is frequency-independent. Frequency-dependent site amplifications are not included in the model. The frequency dependence of attenuation is considered. The amplification and attenuation results are used to help determine source parameters for aftershocks of the October, 1989, Loma Prieta earthquake, aftershocks of the May, 1983, Coalinga earthquake, and earthquakes that occurred in Mammoth Lakes earthquake sequence of May to June, 1980.

It is found that the frequency dependence of attenuation strongly affects the determination of source parameters. A Q that decreases with increasing frequency is more likely to influence the determination of source parameters than one which increases with frequency. A Q that decreases with frequency causes the spectrum to fall off rapidly at high frequencies. The rapid falloff of the spectrum at high frequencies due to attenuation could dominate the high frequencies obscuring source effects. This becomes an important consideration for the phenomenon observed for small earthquakes sometimes referred to as f_{\max} [Hanks, 1982]. A number of studies have found that stress drops of small earthquakes apparently become smaller for lower

moment earthquakes [e.g., Tucker and Brune, 1973; Chouet *et al.*, 1978; Fletcher, 1980; Archuleta *et al.*, 1982; McGarr *et al.*, 1990]. Attenuation has been proposed as a possible cause for biases in the determination of source parameters that might lead to an apparent lowering of stress drops [Hanks, 1979; Frankel, 1982; Anderson, 1986; Frankel and Wennerberg, 1989]. If Q does decrease with frequency, the possibility of attenuation affecting the measurement of source parameters becomes more likely.

In this study we are primarily concerned with attenuation in the near surface. For epicentral distances out to several hundred kilometers, Anderson and Hough [1984] showed that to first approximation attenuation could be separated into a near-surface attenuation and an attenuation at depth. The near-surface attenuation occurs in the top several kilometers through which all ray paths must travel. The present study examines locally recorded earthquakes with epicentral distances that are usually less than about 30 km. For these distances the attenuation is dominated by the near-surface attenuation. Consequently, this study can say little about attenuation at depth.

Papers that have studied the frequency dependence of attenuation of seismic waves for locally recorded earthquakes have not always arrived at the same conclusions. Frankel and Wennerberg [1989] studied earthquakes near Anza, California using small earthquakes as empirical Green's functions. They concluded that their results were consistent with a frequency-independent Q . Hough *et al.* [1988] examined the falloff of the Fourier spectra at high frequencies to determine attenuation also using the Anza data. They concluded that Q increased with increasing frequency. On the other hand, Blakeslee and Malin [1991] calculated spectral ratios of surface to downhole recordings of earthquakes near Parkfield, California. The spectral ratios indicated that Q above approximately 30 Hz was less than Q below about 10 Hz (Q

Copyright 1992 by the American Geophysical Union.

Paper number 92JB00550.
0148-0227/92/92JB-00550\$05.00

decreased with frequency). *Castro et al.* [1990] measured attenuation of earthquakes along the Guerrero subduction zone in Mexico. They found a somewhat complicated frequency dependence of attenuation but with a decrease of Q for S waves from 2 to 20 Hz for some of the sites in the study.

Once a suitable model for amplification and attenuation has been developed, source parameters can be calculated. For this study source parameters were determined for Coalinga, Mammoth Lakes, and the Santa Cruz Mountains, California. An important result of this paper is that stress drops calculated for earthquakes in the Santa Cruz Mountains were lower than stress drops at Coalinga or Mammoth Lakes. Any change of stress drop between the three areas is important because it may indicate fundamental differences in the earthquake rupture process. There are several possible causes for variations of stress drop between the three regions. One possibility is that the stress drop varies with the orientation of the stress field. The stress required for failure based on a Coulomb failure criterion depends on the orientation of the stress field [e.g., *Sibson*, 1974] with highest stress required for thrust earthquakes and lowest stress required for normal earthquakes. It might be expected, therefore, that stress drop would be greatest for thrust faulting such as at Coalinga.

Another possibility is that the stress drop varies due to variations of pore fluid pressure. It has been proposed that pore fluid pressure within the San Andreas Fault Zone is significantly higher than outside the fault [*Rice*, 1990]. This could explain how earthquakes occur on the San Andreas Fault when it appears that the maximum principal stress is almost perpendicular to the fault and that the fault is a weak fault [*Zoback et al.*, 1987]. Lower stress drops within the San Andreas Fault may be an indication of high pore fluid pressure within the fault zone.

DATA

Loma Prieta Aftershocks

Aftershocks of the M_S 7.1 October 17, 1989, Loma Prieta earthquake were recorded in the Santa Cruz Mountains as part of an IRIS/PASSCAL experiment [*Simpson et al.*, 1989]. The earthquakes were recorded by Reftek recorders with Mark Products L-22 2 Hz geophones. Most of the data were recorded at 200 samples/s with a 90 Hz anti-alias filter. Some data were recorded at 100 samples/s with a 45 Hz anti-alias filter. Magnitudes ranged from 1.2 to 4.4 with most magnitudes between 1.5 and 3.2. Locations shown in Figure 1 are from the U. S. Geological Survey. The site geology was either Tertiary sedimentary rocks or Franciscan assemblage [*Clark*, 1970; *Dibblee and Brabb*, 1978, 1980; *Dibblee et al.*, 1978; *Brabb and Dibblee*, 1979].

Coalinga Aftershocks

Aftershocks of the M_L 6.7 May 2, 1983, Coalinga earthquake were recorded by the U. S. Geological Survey [*Mueller et al.*, 1984]. The earthquakes were recorded by GEOS recorders [*Borcherdt et al.*, 1985] with a Mark Products L-22 2 Hz geophone and a Kinometrics FBA-13 accelerometer at each site (Figure 2). Aftershock locations in Figure 2 were taken from *Eberhart-Phillips* [1989]. Because of the better signal to noise ratio, data recorded from the L-22 sensors were used preferentially over recordings from the FBA-13 accelerometers unless the L-22 sensors were off scale. The aftershocks were recorded at 200 samples/s with a 50 Hz anti-

alias filter. For this study we have used a subset of the data consisting of earthquakes recorded at three or more stations. This subset included 129 earthquakes ranging from magnitude 1.9 to 5.3 with most magnitudes between 2.0 and 3.5. The locations of the sites used in this study are shown in Figure 2. The geology of the sites ranged from relatively thick alluvium sites in Pleasant Valley and the San Joaquin Valley to Pliocene age sandstone outcrop sites located on Coalinga Anticline [*Dibblee*, 1971a,b].

Mammoth Lakes Data

Earthquakes were recorded in the Mammoth Lakes area by the U. S. Geological Survey during the May-June 1980 earthquake sequence [*Mueller et al.*, 1981; *Spudich et al.*, 1981]. Earthquake and instrument locations are shown in Figure 3. GEOS recorders were used with either a Mark Products L-22 sensor or a Kinometrics accelerometer at each site. The earthquakes were sampled at 200 samples/s with a 50 Hz anti-alias filter. A total of 470 earthquakes were studied ranging from magnitude 2.8 to 6.4 with most magnitudes between 3.0 and 4.5. Eight sites were used in this study and the geology of the sites was taken from *Bailey* [1989]. Four sites were located within the Sierra Nevada on relatively thin amounts of glacial deposits or Quaternary alluvium above hard rock (granitic, metasedimentary, or volcanic). Two sites were located at the base of the Sierra Nevada on alluvium with unknown but deeper thicknesses to basement. One site was located in the western half of the Long Valley caldera on Pleistocene volcanics of the resurgent dome. A second caldera site was located in the eastern half of the caldera next to Lake Crowley on alluvium with lacustrine deposits nearby.

Range of Frequencies Studied

The range of frequencies that could be analyzed was limited by noise, anti-alias filters, and the response of the instruments. For P waves, the noise was determined for each seismogram from the Fourier spectrum of a window placed just prior to the first P wave arrival. The range of frequencies studied was then determined by comparing the Fourier spectrum of the noise window to the P wave Fourier spectrum. For the recordings from the L-22 sensors, frequencies below the natural frequency of the sensors, 2 Hz, were not used. In general the highest frequency fit was 35 Hz or higher, but frequencies within ten percent of the anti-alias frequency were not used. If the highest frequency of the signal spectrum was not useable to at least 20 Hz because of noise, the spectrum was not included in the analysis. Using these guidelines 632 P wave spectra from Coalinga, 768 P wave spectra from Mammoth Lakes, and 3770 P wave spectra from Loma Prieta were analyzed.

Similar guidelines were used to determine the frequencies to fit for S waves. S waves were first rotated to transverse (SH) based on epicenter and station locations. The noise window for S waves was placed in the P wave coda just in front of the first S wave arrival. The noise (P wave coda) spectrum was generally observed to merge with the transverse S wave spectrum somewhere between 10 and 35 Hz depending on the recording. S wave spectra were not used if it appeared that the P wave coda dominated at frequencies below 10 Hz. Also the S wave spectra from unlocated earthquakes were not used because then it was not possible to rotate to the transverse component. A total of 387 transverse S wave spectra were

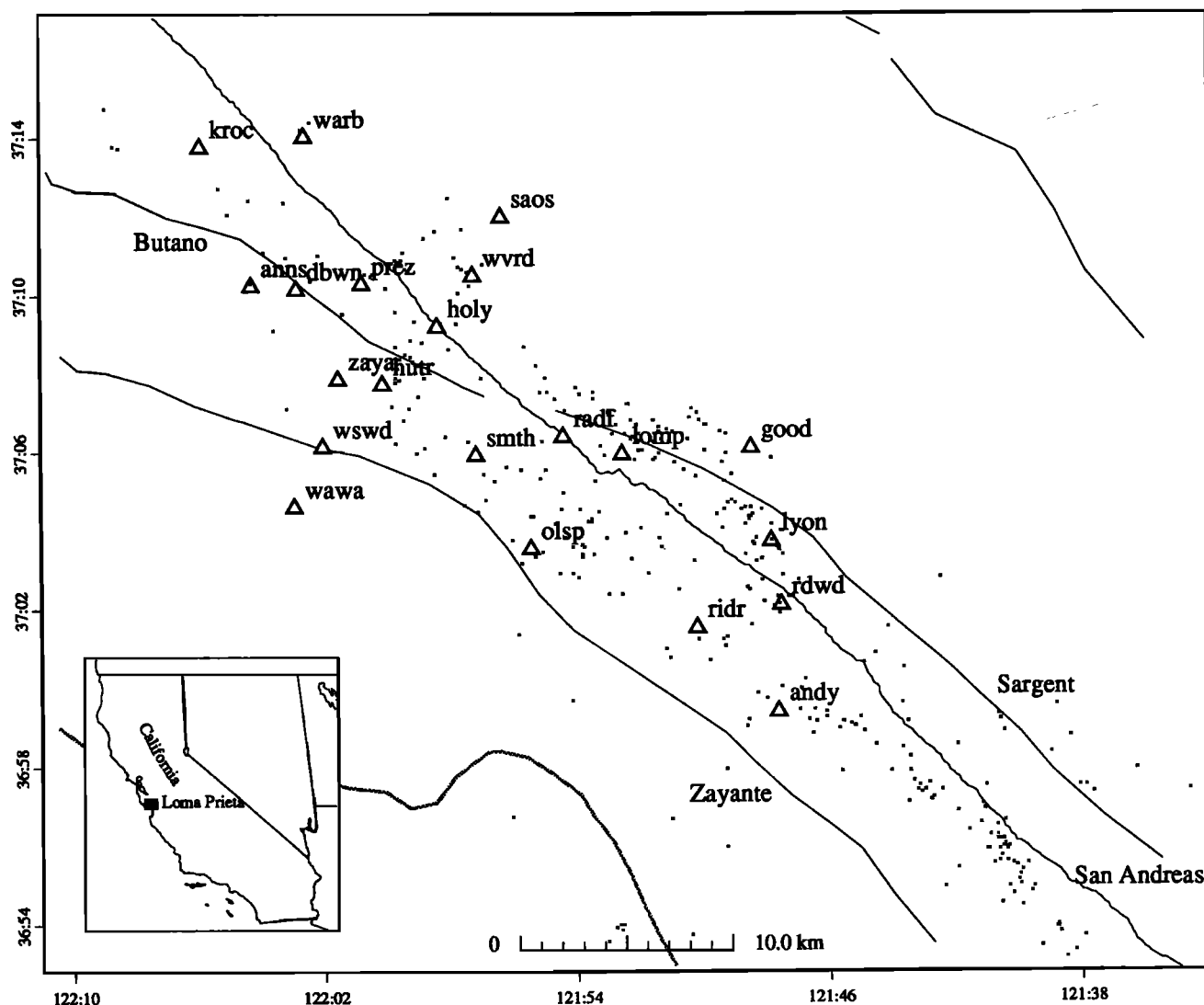


Fig. 1. Locations of instruments and selected aftershocks in the Santa Cruz Mountains, California.

analyzed from Coalinga, 376 transverse *S* wave spectra from Mammoth Lakes, and 2512 from Loma Prieta.

SPECTRAL FITTING METHOD

The Fourier amplitude spectra of *P* and *S* waves were analyzed by finding nonlinear least squares best fits to the spectra. The Fourier spectra were fit to the logarithm of the functional form [Boatwright, 1978]

$$D(f) = \frac{\Omega_0 \exp(-\pi f t^*)}{[1 + (f/f_c)^2 \gamma]^2} \quad (1)$$

$$\log(D(f)) = \log(\Omega_0) - 0.5 \log[1 + (f/f_c)^2 \gamma] - 0.434(\pi f t^*) \quad (2)$$

where $D(f)$ is the Fourier displacement amplitude, Ω_0 is the low-frequency spectral asymptote, f is the frequency, f_c is the corner frequency, γ is the source spectral falloff, and t^* is the travel time divided by the quality factor of attenuation Q . In addition, t^* was determined by two parameters according to $t^* = t_0^* f^{-\alpha}$, where t_0^* and α are parameters determined by the fits. The negative sign was placed before α so that the sign agrees with other attenuation studies which have often used Q

$= Q_0 f^\alpha$ [e.g., Aki, 1980]. The best fit for a particular spectrum is the combination of parameters that minimizes the sum of squared residuals. The residual at each value of the Fourier spectrum is the spectrum minus the fit to the spectrum. The best fitting combination of parameters is identically the same whether fitting to the displacement, velocity, or acceleration spectrum.

The five parameters that can be varied to find the best fits are Ω_0 , f_c , γ , t_0^* , and α . It was impossible to fit to all five parameters at once because there were many possible parameter combinations that produced similar values for the sum of squared residuals. It was usually possible to determine a unique solution when four of the five parameters were allowed to vary. When three of the five parameters were allowed to vary, it was always possible to determine a unique best fitting combination of these three parameters. The fits in this study were usually calculated with the three parameters Ω_0 , f_c , and t_0^* varying and the parameters γ and α fixed. Various values of γ and α were used in the fits, and the results for different values of γ and α were compared to constrain these two parameters.

The best fitting combination of parameters was found by iteration from a starting model using the Simplex algorithm

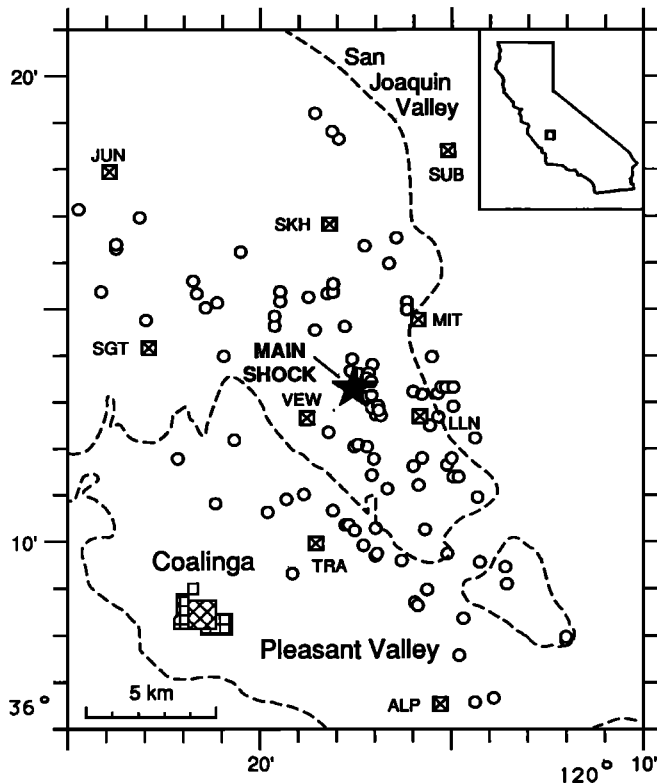


Fig. 2. Locations of aftershocks and instruments near Coalinga, California. Aftershock locations are from Eberhart-Phillips [1989].

[Caceci and Cacheris, 1984; Nelder and Mead, 1965]. The Simplex algorithm has the advantage over many other iteration schemes that convergence toward a minimum value for the sum of squared residuals is guaranteed. Example fits are shown in Figure 4. Smoothing the spectra prior to fitting did not greatly alter the fit parameters. The fit parameters for spectra smoothed by calculating a nine point running mean usually changed by less than 15%.

Analysis of the Fourier spectrum of locally recorded earthquakes by finding least squares best fits to the spectra using the same or a similar source model has been previously studied by a number of authors [Boatwright, 1978; Ihaka, 1985; De Natale et al., 1987; Rovelli et al., 1988; Scherbaum, 1990; Boatwright et al., 1991; Fletcher and Boatwright, 1991]. Other studies that have used automated methods to determine source parameters of local earthquakes include Andrews [1986], Fehler [1985], Snoke [1987], Dysart et al. [1988] and Fehler and Phillips [1991]. The method used in this study differs from these previous studies by using the Simplex algorithm to find the best fitting parameters and by analysing the frequency dependence of attenuation. Fitting the Fourier spectrum using the Simplex algorithm has been used before to find the frequency dependence of attenuation [Walck, 1988]. Walck, however, studied explosions at regional distances rather than local earthquakes as studied in this paper.

FALLOFF OF THE FOURIER AMPLITUDE SPECTRUM

In order to determine an appropriate model that describes the Fourier spectrum of local earthquakes it is necessary to understand the falloff of the spectrum at high frequencies. The

falloff of the Fourier spectrum at high frequencies is due to both the source and attenuation. It is difficult to separate these two effects, especially since attenuation may be frequency dependent. In this study the separation of source from attenuation was accomplished by looking at sites with a wide range in near-surface rock types and therefore a wide range in site attenuation. Station locations with low attenuation were used to constrain the parameter γ which determines the falloff of the spectrum due to the source. Sites with high attenuation were used to determine the frequency dependence of attenuation as modelled by the parameter α .

Source Spectral Falloff

The parameter γ determines the falloff of the spectrum due to the source which for frequencies sufficiently far above the corner frequency goes as $f^{-\gamma}$. The falloff of the spectrum due to attenuation is determined by the parameter t_0^* . Constraints can be placed on γ by considering the average value of the parameter t_0^* for different values of γ . As γ is increased more of the falloff of the spectrum at high frequencies is taken up by γ and less by t_0^* . Eventually this causes t_0^* to go to zero because all of the falloff is taken up by the parameter γ . Because it is physically impossible for t_0^* to be negative the value of γ for which t_0^* is zero can be used as an upper bound on γ . The parameter t_0^* goes to zero for P waves at the lowest attenuation sites when γ approaches 2.5 (Table 1). The parameter γ is therefore less than approximately 2.5. Since t^* is greater for S waves than P waves, it was not possible to use the same method to place significant constraints on the source falloff of S waves, but γ was assumed to be 2.0 for both P and S waves. The value of 2.0 is often used for γ [e.g., Aki, 1967; Brune, 1970; Hanks, 1979].

Frequency Dependence of Attenuation

The frequency dependence of attenuation was determined by the parameter α ($t^* = t_0^* f^{-\alpha}$ or equivalently, $Q = Q_0 f^\alpha$). In general, negative values of α were found to minimize the sum of squared residuals. Examples of spectral fits for different values of α are shown in Figure 4. In Figure 4, negative values of α produce spectral fits that are concave down similar to the data; positive values of α produce spectral fits that are

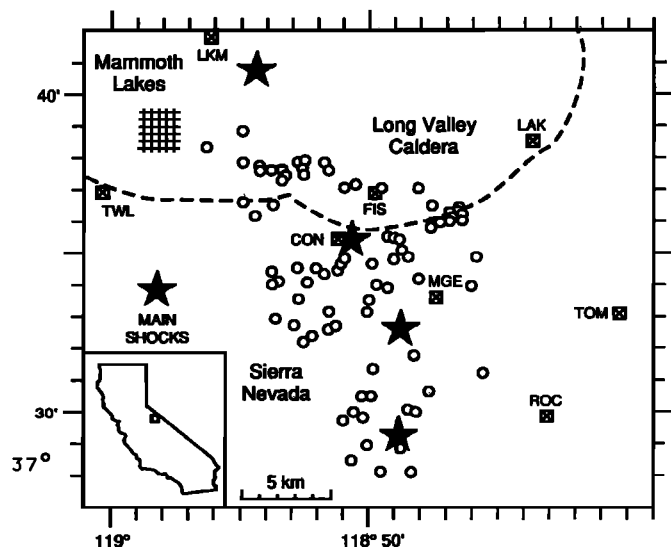


Fig. 3. Locations of earthquakes and instruments near Mammoth Lakes, California.

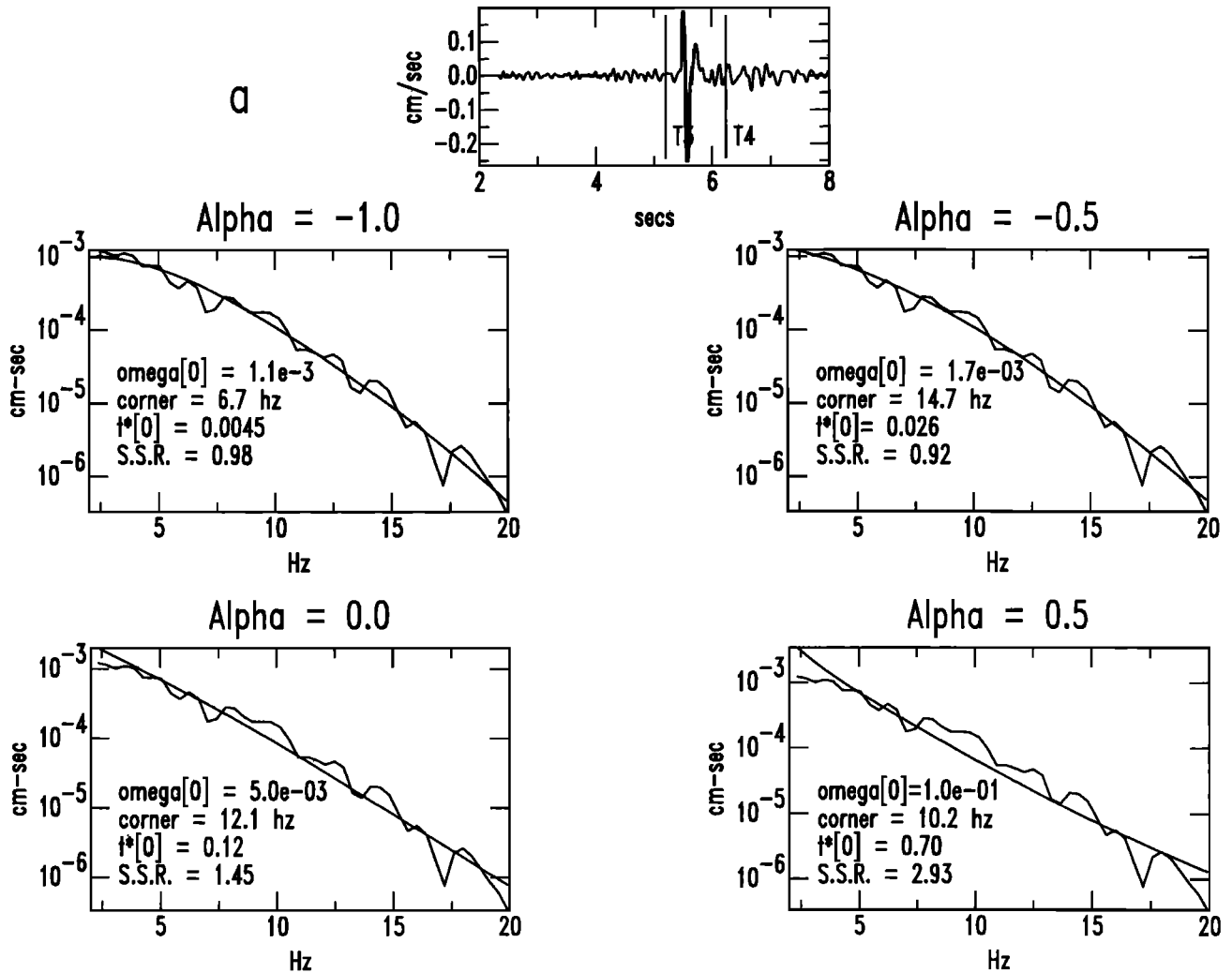


Fig. 4. Example fits for different values of α . T3 and T4 mark the window for which the fast Fourier transform was calculated. All windows were tapered with a 10% cosine taper. The parameter γ was fixed to be 2.0. S.S.R. in the figure is the sum of squared residuals. Best fits were obtained for negative values of α . (a) Fit to S wave spectrum at site TRA, Coalinga, origin time May 6, 11 51:44, $36^{\circ} 15.62' N$, $120^{\circ} 21.73' W$. (b) Fit to P wave spectrum at site SMTH, Santa Cruz Mountains, origin time October 22, 2 54:29, $37^{\circ} 4.20' N$, $121^{\circ} 53.81' W$.

concave up. For α equal to zero, the spectral fits are concave down, but do not have as much curvature as the spectra. For negative values of α , t^* increases with frequency (Figure 5). This increase of t^* with frequency produces the concave downward appearance of the fits that allows the fits to match the spectra.

The results can be compared between sites by plotting the average squared residual per point versus α (Figure 6). High and moderate attenuation sites are shown in the top two plots of Figures 6a and 6b. Low attenuation sites are shown in the bottom plots of Figures 6a and 6b. For P waves at the moderate and high attenuation sites, the best fitting value of α changes from site to site but is typically -0.5 or -0.75. For S waves the minima are usually broader, but again the best fitting values of α are generally negative. For α equal to 0.5, the fit to the data is much worse than for negative values of α . For α equal to zero, the fit to the data is slightly worse than the fit for negative values of α . For the low attenuation sites, α is usually poorly resolved from the data.

Because of the small strains for most of the earthquake

recordings in this study, the attenuation should be linear in amplitude. In order to test this, t_o^* was plotted versus Ω_o (Figure 7). For α equal to 0.5, t_o^* increases strongly with Ω_o . Since it is unlikely that attenuation is really nonlinear for these small earthquakes, this result indicates that site and source effects were not properly separated from the spectra when the fits were calculated with α equal to 0.5. When α is zero, t_o^* increases less strongly with Ω_o , but still increases. For negative values of α , t_o^* is nearly independent of Ω_o , as would be expected if site and source effects were properly separated by the fit parameters.

VARIATION OF ATTENUATION AND AMPLIFICATION WITH SITE GEOLOGY

Values of t_o^* did not vary greatly with distance for most of the sites in this study (Figure 8). This indicates that attenuation occurs primarily in the near surface for these short epicentral distances. The average t^* values varied by up to a factor of 10 between sites for both P and S waves. Values of

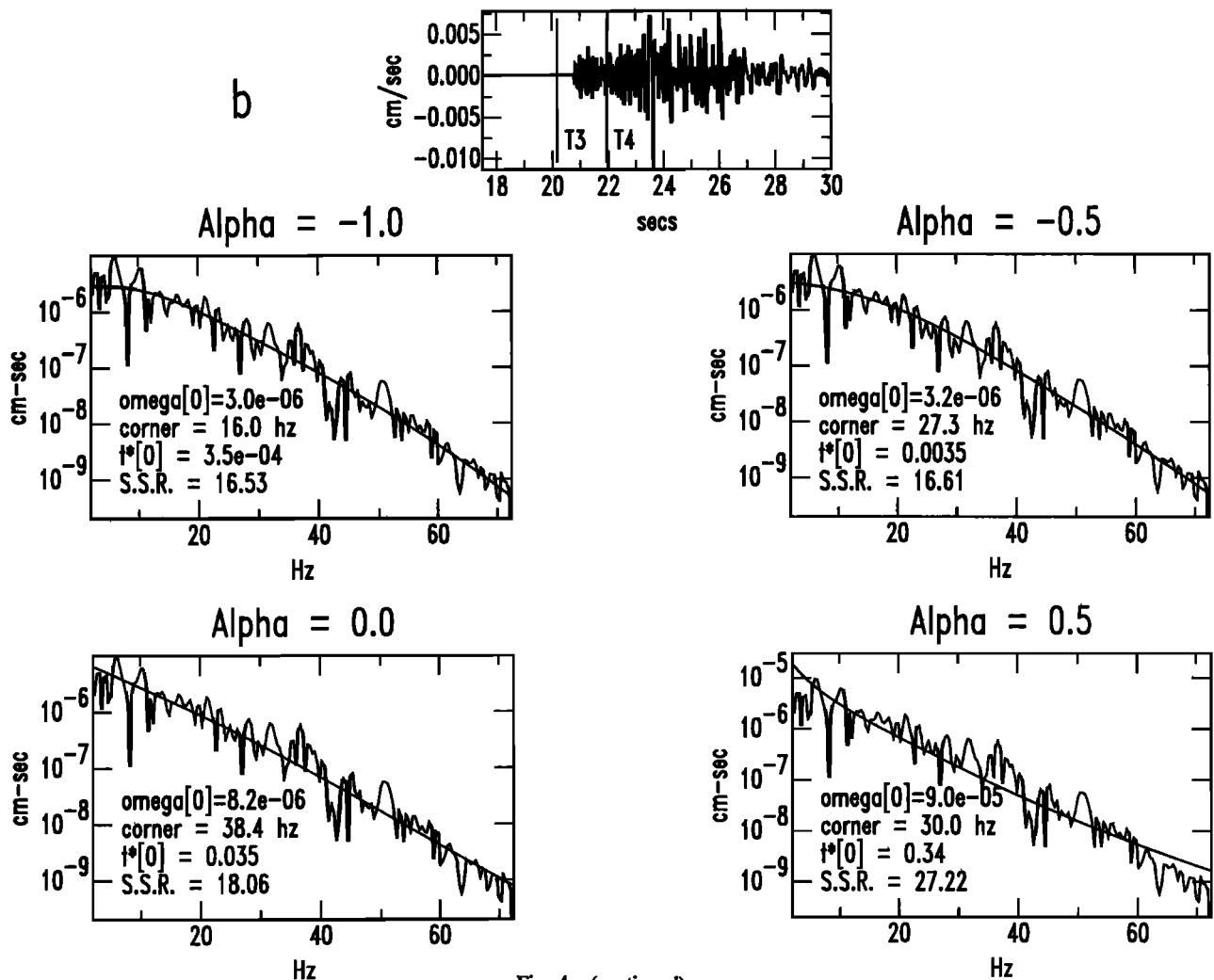


Fig. 4. (continued)

t^* were smallest at sites in the Sierra Nevada near Mammoth Lakes and highest at sites on alluvium near Coalinga (Figure 9 and Table 2).

The relative amplification between sites varied by about a factor of 5 within each region and also correlates with site geology (Figure 9 and Table 3). The relative amplification between sites was determined by first calculating the log average ratio of the low-frequency spectral asymptote between each site according to

$$R_{ij} = \left[\sum_{k=1}^n \log(\Omega_{oi}^k / \Omega_{oj}^k) \right] / n \quad (3)$$

Where R_{ij} is the relative amplification of site i compared to site j , Ω_{oi}^k is the low-frequency asymptote for the k^{th} earthquake at station i , and n is the number of earthquakes recorded in common between the two sites. The Ω_o values were normalized to 10 km hypocentral distance by assuming straight line ray paths. An average relative amplification was then calculated for each site by averaging the R_{ij} :

$$A_i = \left[\sum_{j=1}^N R_{ij} \right] / N \quad (4)$$

where A_i is the relative amplification at site i and N is the number of sites.

TABLE 1. Average P Wave t^* Values for Different Values of γ

Site	No. of Fits	t^* for $\gamma = 2.0$	t^* for $\gamma = 2.5$	t^* for $\gamma = 3.0$
ROC	62	0.0048 \pm 0.0012	-0.0011 \pm 0.0012	-0.0049 \pm 0.0014
MGE	54	0.0061 \pm 0.0016	0.0005 \pm 0.0017	-0.0009 \pm 0.0023
CON	24	0.0084 \pm 0.0020	0.0042 \pm 0.0021	-0.0022 \pm 0.0023
TWL	19	0.0013 \pm 0.0032	-0.0003 \pm 0.0035	-0.0002 \pm 0.0031
Average	159	0.0050 \pm 0.0011	0.0002 \pm 0.0011	-0.0015 \pm 0.0012

Here, t^* approaches zero for γ equal to 2.5, implying γ is less than approximately 2.5; t^* values were calculated with α equal to 0.0, but similar results are obtained for other values of α . Errors are the standard deviation of the mean.

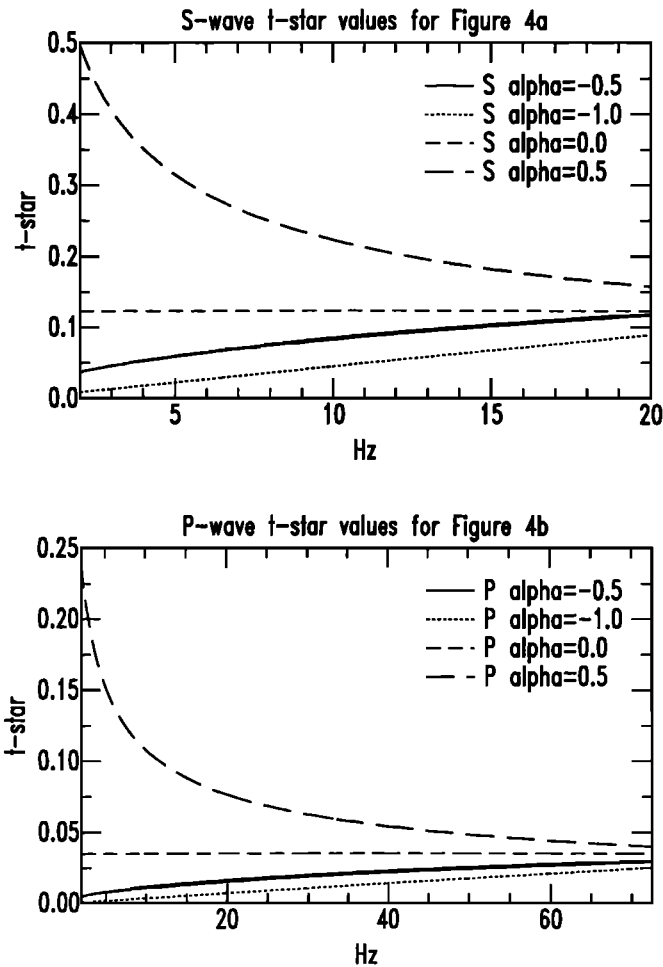


Fig. 5. Variation of t^* with frequency for fits in Figure 4. At high frequencies, t^* is nearly equal for the different values of α . Large differences in t^* occur at lower frequencies.

In the Santa Cruz Mountains, sites on Franciscan assemblage had the lowest amplification and attenuation (Figure 9 and Tables 2 and 3). Attenuation and amplification also varied among the Tertiary sedimentary rock sites and were on average larger for the younger age rocks (Pliocene and Miocene) compared to the older (Oligocene and Eocene) sites (Table 3).

At Coalinga the largest amplification and attenuation occurred at the alluvium sites (ALP, TRA, and SUB). The alluvium sites had t^* values about twice the nearby sedimentary rock sites and were amplified on average by a factor of 4 or 5 (Figure 9 and Table 2). The amplification cannot be compared directly between the three areas, since it is a relative amplification between sites, but the attenuation can be compared. The attenuation at the Coalinga sedimentary rock sites is similar to the highest attenuation sites in the Santa Cruz Mountains (Figure 9 and Table 2). This is reasonable, since the age of the Coalinga sedimentary rock sites is Pliocene, and the highest attenuation sites in the Santa Cruz Mountains were usually Pliocene or Miocene. Site JUN at Coalinga had unusually large amplification and attenuation for a sedimentary rock site. It is the only site to sit on Cretaceous age rocks at Coalinga and presumably the properties of these sedimentary rocks are substantially

different from the Tertiary sedimentary rock sites at Coalinga and in the Santa Cruz Mountains.

The largest attenuation in the Mammoth Lakes area occurred at site LAK in the southeastern end of the Long Valley Caldera, where a large thickness of unconsolidated sediments would be expected. The attenuation for the caldera sites (LAK and LKM) is roughly equivalent to the sedimentary rock sites at Coalinga and the Santa Cruz Mountains. On average the lowest values of t^* measured in this study occurred within the Sierra itself (MGE, CON, TWL, and ROC). As in the other regions, there is a large variation in site amplification at Mammoth Lakes, however, amplification does not correlate as well with site geology as in the other regions.

SOURCE PARAMETERS

Moment versus corner frequency plots for P and S waves in all three regions are shown in Figure 10. Lines of constant stress drop for S waves were calculated using the equation [Brune, 1970, 1971]

$$\Delta\tau = 7/16 (2\pi f_c / 2.34\beta)^3 M_0 \quad (5)$$

where $\Delta\tau$ is the stress drop, β is the shear wave velocity, and M_0 is the seismic moment. The moments for S waves were determined by

$$M_0 = 4\pi (\rho_s^{1/2} \rho_r^{1/2}) (\beta_s^{5/2} \beta_r^{1/2}) r \Omega_0 / 2R\theta\phi \quad (6)$$

where ρ_s and β_s are the density and velocity at the source, ρ_r and β_r are the density and velocity at the receiver, and r is the hypocentral distance. The value of $R\theta\phi$ is determined by the radiation pattern and was taken to be 0.55 for S waves and 0.33 for P waves [Boore and Boatwright, 1984]. The factor of 2 in the denominator of equation (6) accounts for amplification at the free surface. The shear wave velocity was taken to be 3.5 km/s and the density 2.9 g/cm³ at the source and 700 m/s and 2.4 g/cm³ at the surface. The P wave velocity was assumed to be $\sqrt{3}$ times the S wave velocity. The moments were also divided by the relative site amplification (Figure 9) in order to account for the different amplification and velocity at each site. The lines of constant stress drop for P waves were plotted using equations from Trifunac [1972], which are similar to the S wave calculations.

It has been shown that measurements of source parameters from a single Fourier spectrum have large errors associated with them [Hough et al., 1991]. The source parameters shown in Figure 10 are log averages [Archuleta et al., 1982] over four or more spectra for Coalinga and Mammoth Lakes. For the Santa Cruz Mountains, earthquake source parameters were determined from log averages of at least six spectra and up to as many as 18 spectra. Source parameters and the errors associated with them for selected P waves from Loma Prieta aftershocks are shown in Table 4. Of 287 earthquakes, the largest stress drop at Loma Prieta was determined for the earthquake that occurred on October 22 at 09:44:58 (Table 4). This earthquake was located within the errors of measurement at the same hypocenter as the April 18, M_L 5.4 Watsonville earthquake. Hough et al. [1991] also found the October 22 earthquake to have an unusually large stress drop.

An important result is that the calculated source parameters change significantly depending on the frequency dependence of attenuation (Figure 10). The variation of the source

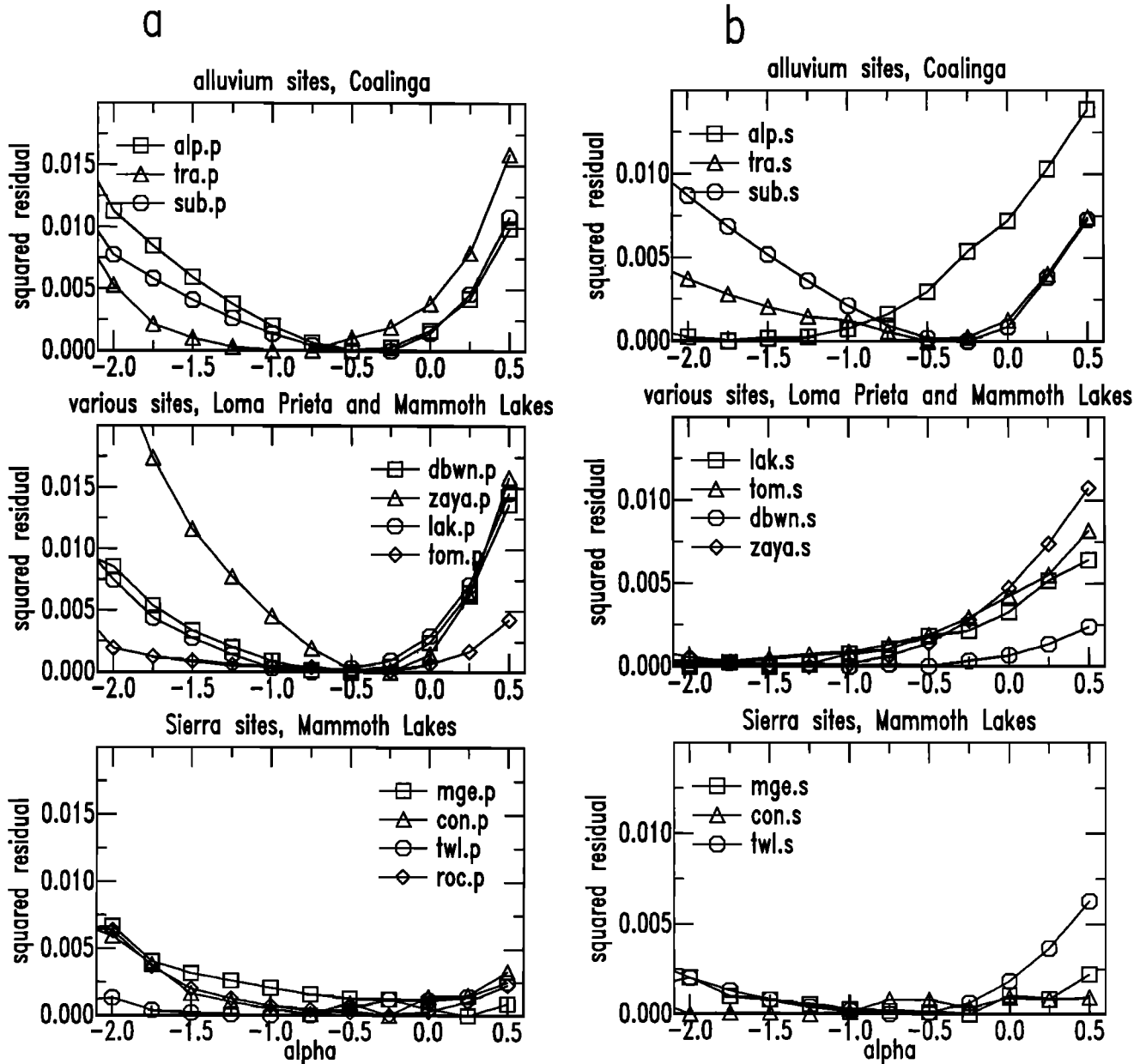


Fig. 6. Variation of the average squared residual per point versus α for various sites. (a) P waves and (b) S waves. The top plot shows the high attenuation alluvium sites at Coalinga. The middle plot shows various sites at Coalinga and Loma Prieta. The bottom plot shows the low attenuation sites within the Sierran batholith. A constant has been removed from the average squared residual for each site so that the average squared residual is zero at the best fitting value of α . This allows multiple sites to be plotted on the same graph. The best fitting value of α is generally less than zero and varies from site to site. The parameter α is poorly resolved for the low attenuation sites in the Sierra Nevada.

parameters with α is similar for all three regions and for both P and S waves. For α equal to 0.5, there is large scatter in the results with a number of unphysically high stress drops, some over 1000 MPa. These plots show the poor nature of the results when α is positive. The plots for $\alpha = 0.0$ are more reasonable, but there is still a lot of scatter and many high stress drop earthquakes. When α is -0.5, the moments have a consistent f_c^3 trend that corresponds to an approximate constant average stress drop with moment. Stress drop values are also more physically reasonable when α is less than zero. For $\alpha = -1.0$, the results are similar to the $\alpha = -0.5$ plots except that the stress drops are somewhat smaller and the variation in stress drops is slightly reduced.

Despite the similarities between the three regions, there are

some significant differences between the source parameters measured at Coalinga and Mammoth Lakes and the source parameters measured at the Santa Cruz Mountains. Both the seismic moments and stress drops were smaller for Loma Prieta aftershocks compared to Coalinga or Mammoth Lakes. The moments at Coalinga and Mammoth Lakes ranged from roughly 5×10^{12} to 10^{15} Nm with one earthquake at Coalinga that had a moment slightly greater than 10^{16} Nm. The moments at Loma Prieta ranged from about 2×10^{11} to 3×10^{14} Nm. The corner frequencies at Loma Prieta were on average larger than the corner frequencies at Coalinga or Mammoth Lakes (Figure 10). However, because of the smaller seismic moments, the stress drops at Loma Prieta were lower by about a factor of 5 than the stress drops at Coalinga or Mammoth

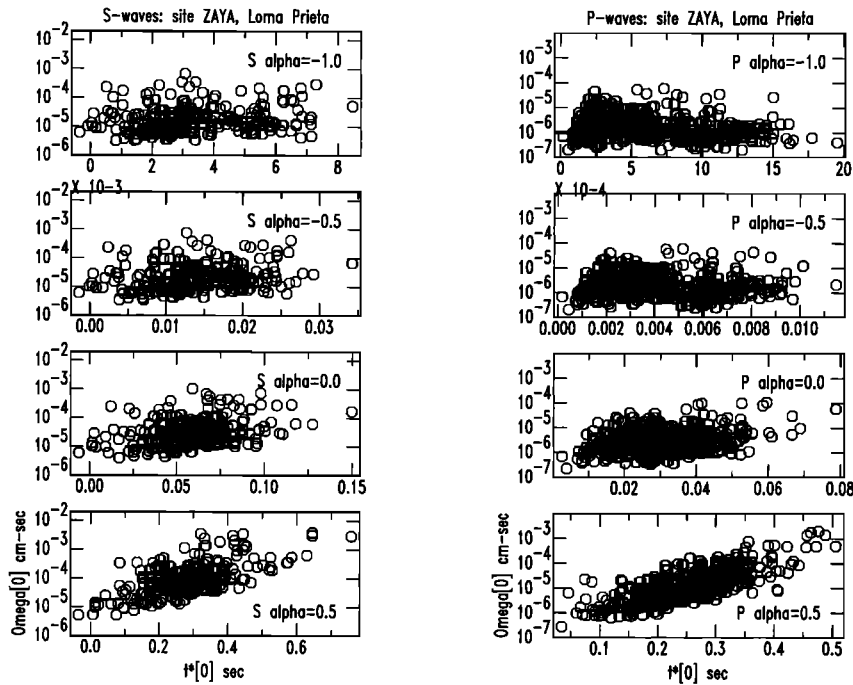


Fig. 7. Ω_0 versus t_0^* for different values of α at site ZAYA, Santa Cruz Mountains. The t_0^* values vary systematically with Ω_0 when α is positive or zero. Only for negative values of α is t_0^* independent of Ω_0 .

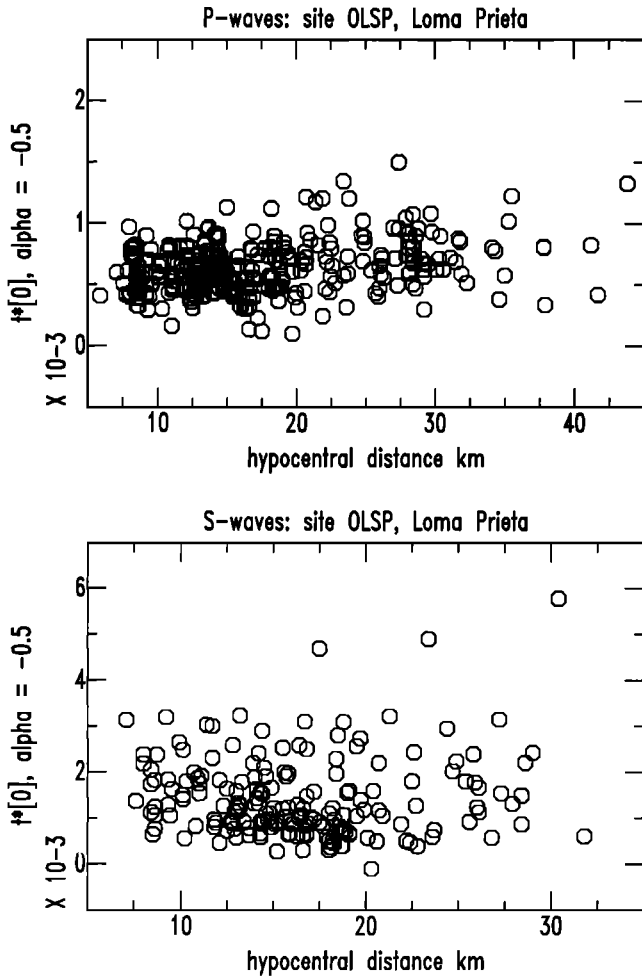


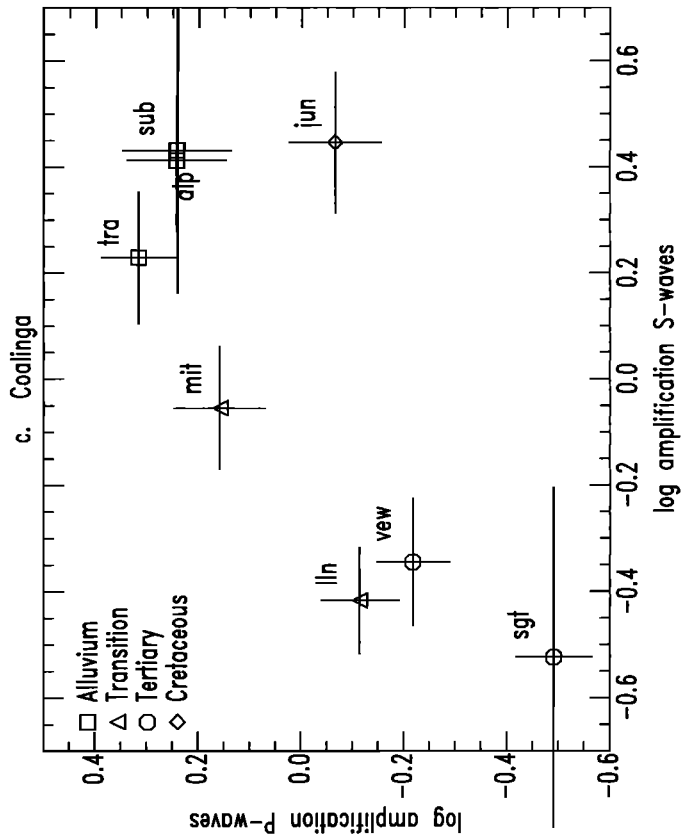
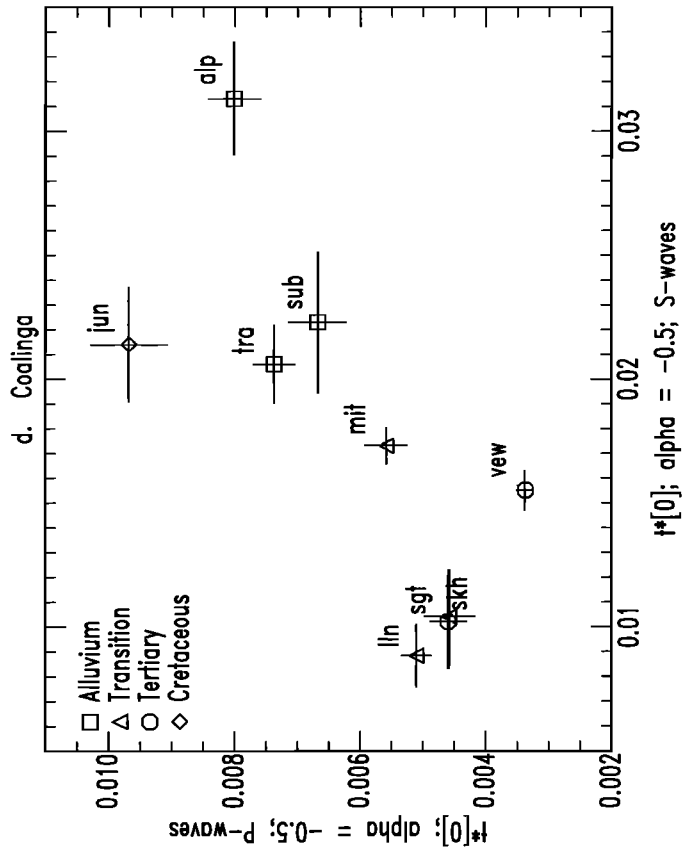
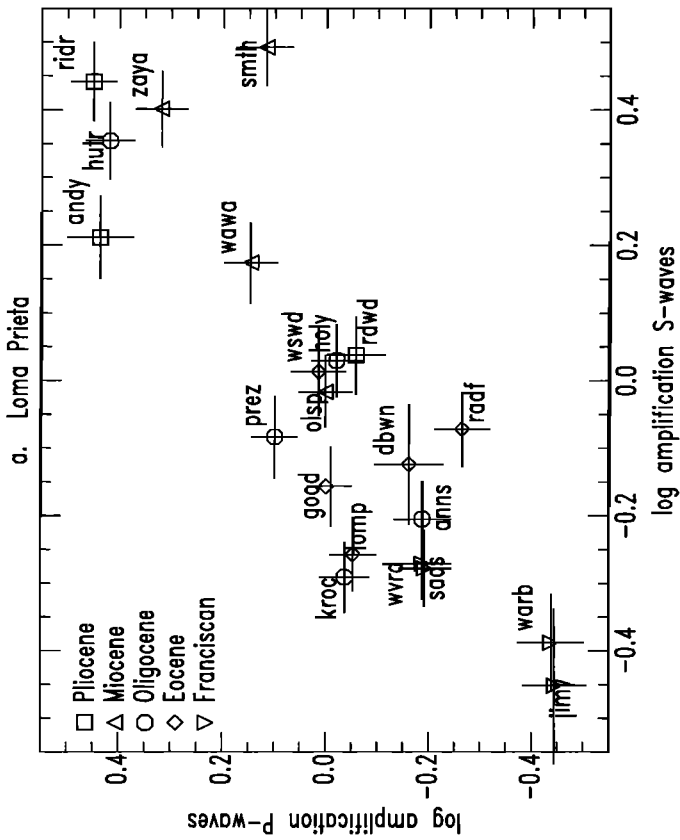
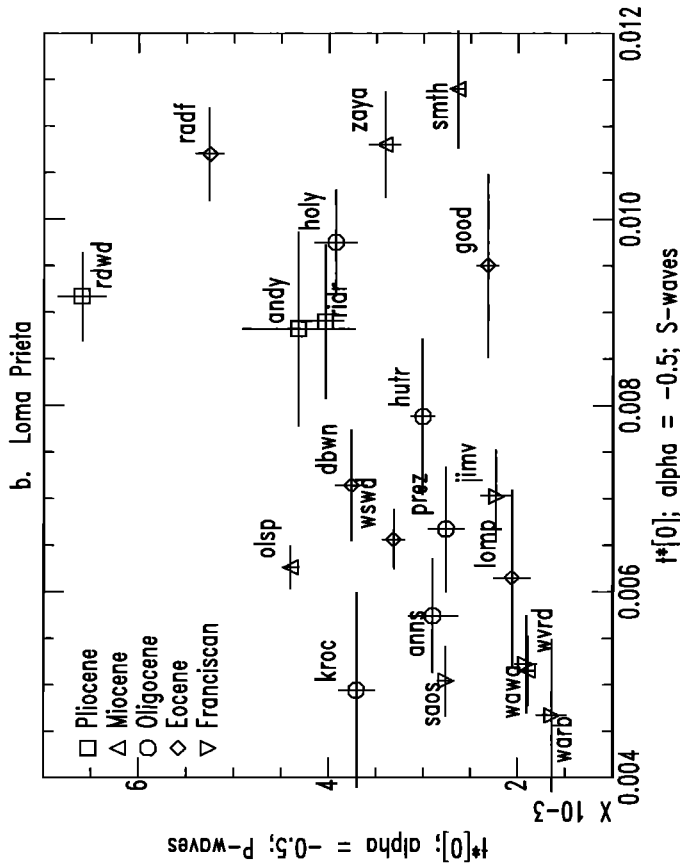
Fig. 8. Variation of t_0^* with hypocentral distance for site OLSP, Santa Cruz Mountains. The t_0^* values were calculated with α equal to -0.5. There is large scatter in the t_0^* values, but only a slight increase in t_0^* with distance, indicating that most of the attenuation occurs in the near surface.

Lakes. For $\alpha = -0.5$, stress drops at Loma Prieta varied from approximately 0.05 to 8.0 MPa, while at Coalinga and Mammoth Lakes the stress drops varied from approximately 0.2 to 50 MPa. Another difference between Loma Prieta and the other two regions is the P to S wave corner frequency ratio. For $\alpha = -0.5$ at Coalinga, the ratio is $1.29^{+0.05}_{-0.05}$ (log average of 374 ratios), and at Mammoth Lakes the ratio is $1.44^{+0.11}_{-0.09}$ (185 ratios) in reasonable agreement for the two regions. The ratio is much higher for the Santa Cruz Mountains ($2.05^{+0.03}_{-0.02}$ for 2222 ratios).

DISCUSSION

This study was initiated to determine if an f^{-2} source falloff and a constant Q with frequency could be used to fit the Fourier spectra of earthquakes. It was found that there was a systematic misfit between this model and the Fourier spectra (Figure 4). This misfit was removed by using a Q that decreased with increasing frequency. This frequency dependence for Q gave better fits to the data (Figures 4 and 6), produced attenuation that did not vary systematically with the low-frequency spectral asymptote (Figure 7), and yielded more reasonable source parameters (Figure 10). We still need to address more carefully whether the apparent frequency dependence of attenuation measured in this study could be due to other causes, either a source effect or a site effect rather than attenuation.

A decreasing Q with frequency was necessary to fit the data because it allowed for a rapid falloff of the fits at high frequencies while leaving the fits at low frequencies relatively flat. It is difficult to explain this rapid falloff at high frequencies as a source effect. The source falloff was directly limited, at least for P waves, by the nearly hard rock sites located in the Mammoth Lakes region where the falloff of the spectrum was close to $f^{-2.5}$ (Table 1). A more general indication that the rapid falloff at high frequencies is due to a site effect rather than a source effect is that the falloff varies



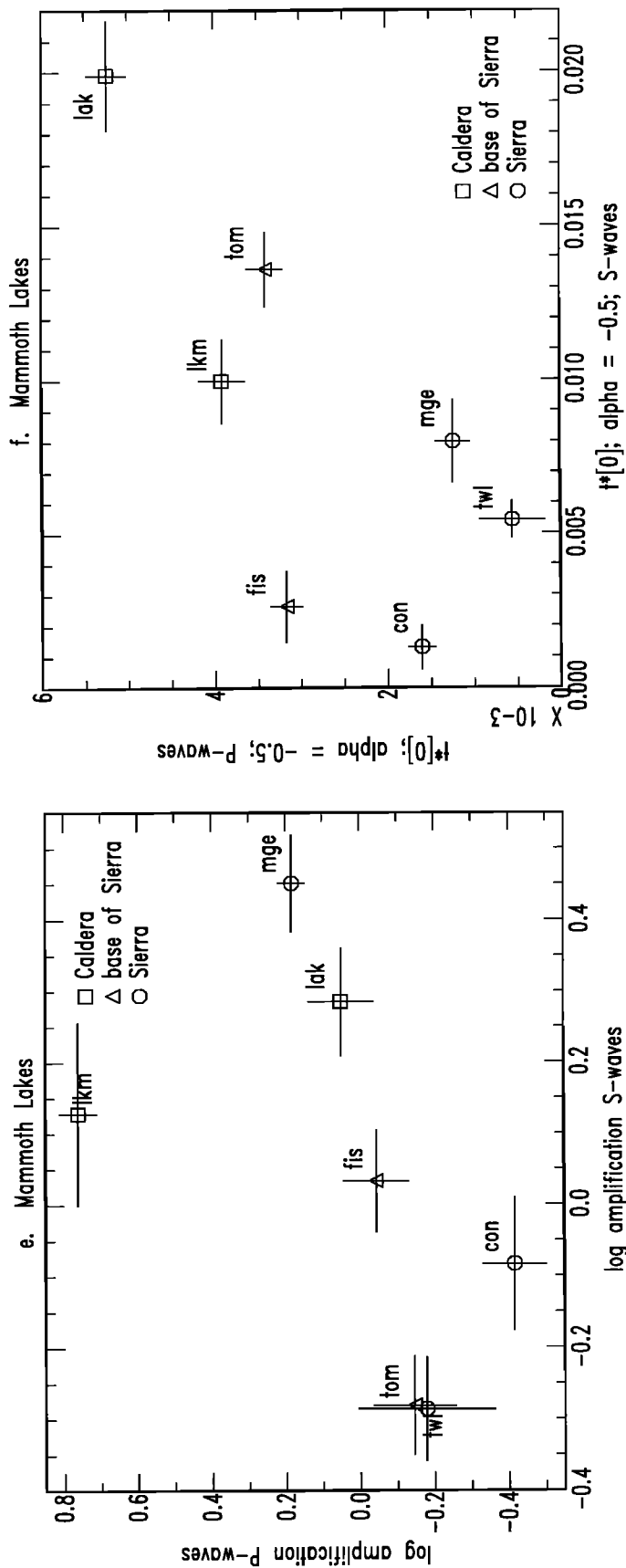


Fig. 9. *S* and *P* wave amplification and attenuation. Values of t_0^* are averages for events within 20 km of each site. Amplification is the relative site amplification. See text for an explanation of this calculation. (a) Amplification in the Santa Cruz Mountains; (b) attenuation in the Santa Cruz Mountains; (c) amplification at Coalinga; (d) attenuation at Coalinga; (e) amplification at Mammoth Lakes; (f) attenuation at Mammoth Lakes.

TABLE 2. *P* and *S* Wave t^* Values for Frequency-Independent Attenuation

Site Geology	Site Name	<i>S</i> wave t^* , s	<i>P</i> wave t^* , s
Alluvium: Coalinga	ALP	0.119 ± 0.007 (25)	0.051 ± 0.002 (40)
	TRA	0.089 ± 0.006 (53)	0.050 ± 0.002 (83)
	SUB	0.092 ± 0.011 (15)	0.045 ± 0.003 (26)
Tertiary Sedimentary: Coalinga and Loma Prieta	MIT	0.075 ± 0.003 (56)	0.038 ± 0.002 (72)
	SGT	0.044 ± 0.007 (18)	0.035 ± 0.002 (47)
Franciscan Assemblage: Loma Prieta	ZAYA	0.046 ± 0.002 (106)	0.025 ± 0.001 (160)
	SMTH	0.054 ± 0.003 (101)	0.026 ± 0.001 (129)
	SAOS	0.024 ± 0.002 (69)	0.022 ± 0.001 (112)
	WARB	0.027 ± 0.003 (50)	0.014 ± 0.001 (59)
	WVRD	0.024 ± 0.002 (101)	0.017 ± 0.001 (123)
Sierran Batholith Mammoth Lakes	JIMV	0.032 ± 0.002 (20)	0.018 ± 0.001 (39)
	CON	0.007 ± 0.003 (59)	0.013 ± 0.001 (74)
	ROC	—	0.008 ± 0.001 (170)
	MGE	0.042 ± 0.005 (39)	0.010 ± 0.002 (81)
	TWL	0.029 ± 0.003 (55)	0.004 ± 0.002 (26)

Here, t^* was calculated for events within 20 km hypocentral distance of each site. *S* and *P* wave t^* values correlate with site geology. This table can be used to compare results to other studies of near-surface attenuation that have assumed a frequency-independent attenuation. This table can also be used as a starting point to estimate near-surface attenuation based on the site geology. The numbers in parentheses are the number of fits averaged for each t^* . Errors are the standard deviation of the mean.

strongly depending on the site. The rate of the falloff of the spectrum faster than f^{-2} was measured by the parameter t_0^* of the fits. Values of t_0^* varied consistently with site geology (Figure 9 and Tables 2 and 3). The falloff of the spectrum was greatest for alluvium sites near Coalinga and smallest for sites within the Sierran batholith. The rapid falloff of the spectrum at high frequencies is therefore most easily explained as a site effect.

The major deficiency of the model used in this study is that it does not consider frequency-dependent site amplifications. To include parameters for this effect would have required too many parameters in the model to find unique fits to each spectrum. One type of frequency-dependent site amplification is caused by resonances in near-surface layers. These resonances are probably the major source of error in the determination of the corner frequency [Crawswick *et al.*, 1985]. However, it does not seem likely that resonances have caused the frequency dependence of attenuation measured in the present study. Each resonance acts over a relatively short frequency range (a few Hz), whereas the observed frequency dependence of attenuation is the result of the overall shape of the spectrum (a few tens of Hz).

Frequency-dependent site effects that act over a broader frequency range than resonances are also possible. For example, the amplification due to the impedance contrast in the near surface occurs only for high frequencies. Low frequencies will not feel the effects of the near-surface velocity reduction and will be amplified by only the factor of 2 for the free surface [e.g., Shearer and Orcutt, 1987]. We have assumed that the frequencies (all greater than 2 Hz) in this study are sufficiently high that the entire frequency band is amplified by the impedance contrast. For sites where this is not true, the determination of the frequency dependence of attenuation could be biased. The observed variation of amplification with site geology implies that the spectra studied are in the high-frequency limit where there is amplification due to the impedance contrast since the amplification was determined from the low-frequency asymptote (equations (2) and (3)). Frequency-dependent site amplifications can be quite complicated, however, and we cannot eliminate the possibility that frequency-dependent site amplifications are biasing the frequency dependence of attenuation measured in this study.

A near-surface Q that decreases with increasing frequency

TABLE 3. Attenuation and Amplification for Loma Prieta Aftershocks

Site Geology	<i>P</i> wave t_0^* ($\alpha=-0.5$)	<i>S</i> wave t_0^* ($\alpha=-0.5$)	<i>P</i> wave Amp.	<i>S</i> wave Amp.
Pliocene and Miocene	0.0039 ± 0.0001	0.0087 ± 0.0002	1.59 ^{+0.08} _{-0.07}	1.77 ^{+0.09} _{-0.09}
Oligocene and Eocene	0.0033 ± 0.0001	0.0075 ± 0.0003	0.96 ^{+0.05} _{-0.04}	0.83 ^{+0.04} _{-0.03}
Franciscan	0.0021 ± 0.0001	0.0055 ± 0.0003	0.48 ^{+0.04} _{-0.03}	0.45 ^{+0.04} _{-0.04}

Values of t_0^* were calculated with α equal to -0.5 and are averages for all earthquakes within 20 km hypocentral distance of each site. The amplification is the relative amplification between sites. See text for an explanation of this calculation. Franciscan sites include JIMV, SAOS, WARB, and WVRD. Oligocene and Eocene sedimentary rock sites include KROC, PREZ, ANNS, HOLY, HUTR, DBWN, GOOD, LYON, WSWD, RADF, and LOMP. Pliocene and Miocene sites are RDWD, RIDR, ANDY, ZAYA, OLSF, WAWA, and SMTH. Errors are the standard deviation of the mean.

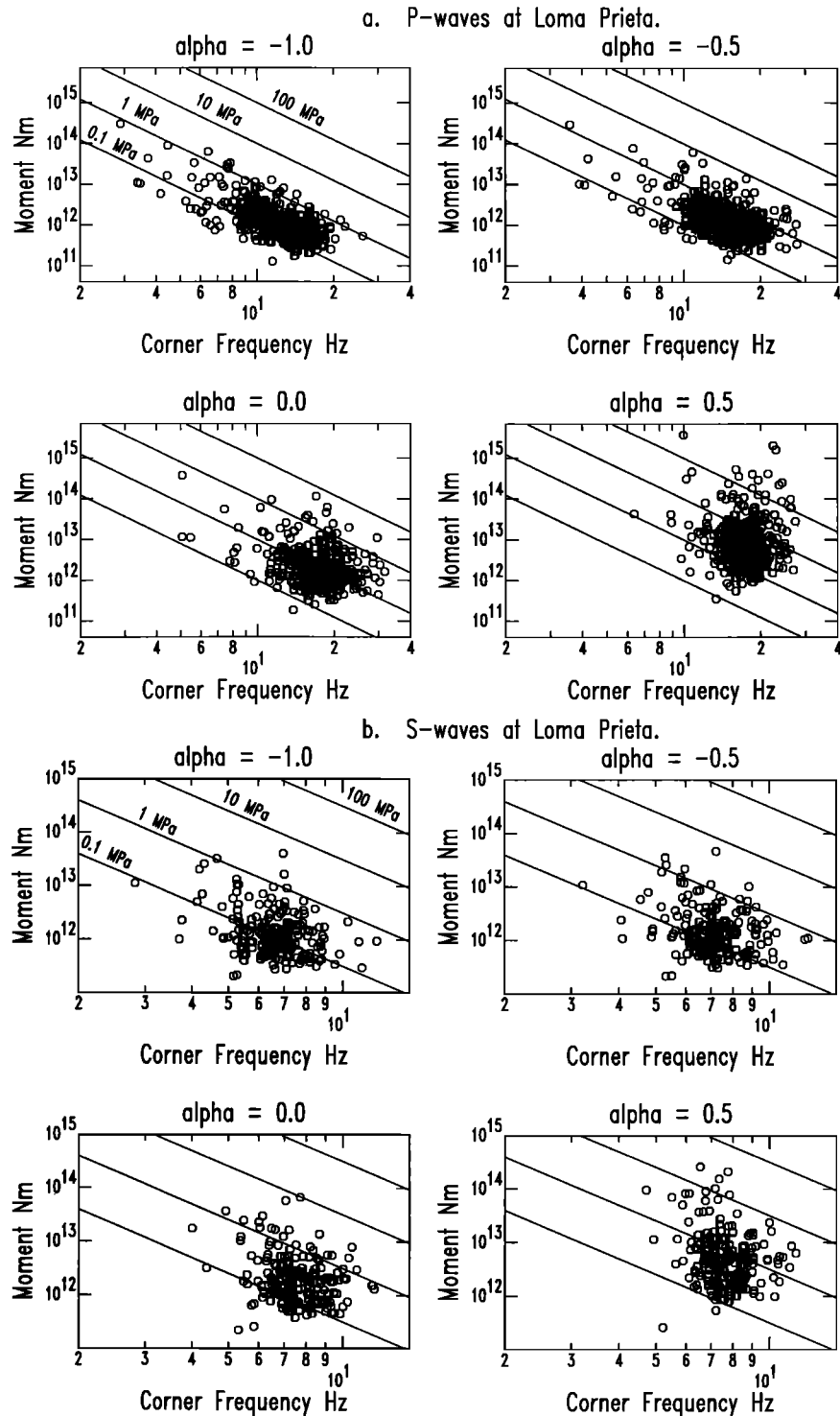


Fig. 10. Moment versus corner frequency plots. Lines of constant stress drop are from *Brune* [1970, 1971] (*S* waves) and *Trifunac* [1972] (*P* waves). For negative values of α , the seismic moments trend approximately as f_c^{-3} .

has been observed before. *Blakeslee and Malin* [1991] averaged spectral ratios of surface to downhole recordings of microearthquakes at two sites near Parkfield, California in order to determine the site effect. The downhole instruments were at approximately 200 m depth. They found what appeared to be a bimodal behavior for Q . Below about 10 Hz, Q was high enough not to have a noticeable impact on the spectral ratios. Above approximately 30 Hz, Q was quite low (between six and 19). This decrease of Q with increasing

frequency is in at least qualitative agreement with the present study.

Many studies of near-surface attenuation have used a frequency-independent Q . In order to facilitate comparisons to these studies, values of t^* for frequency-independent Q have been compiled in Table 2. For example, *Frankel and Wennerberg* [1989] found *S* wave t^* values near Anza, California that varied from approximately 0.01 to 0.05 s. The Anza sites were located within a granitic batholith, and

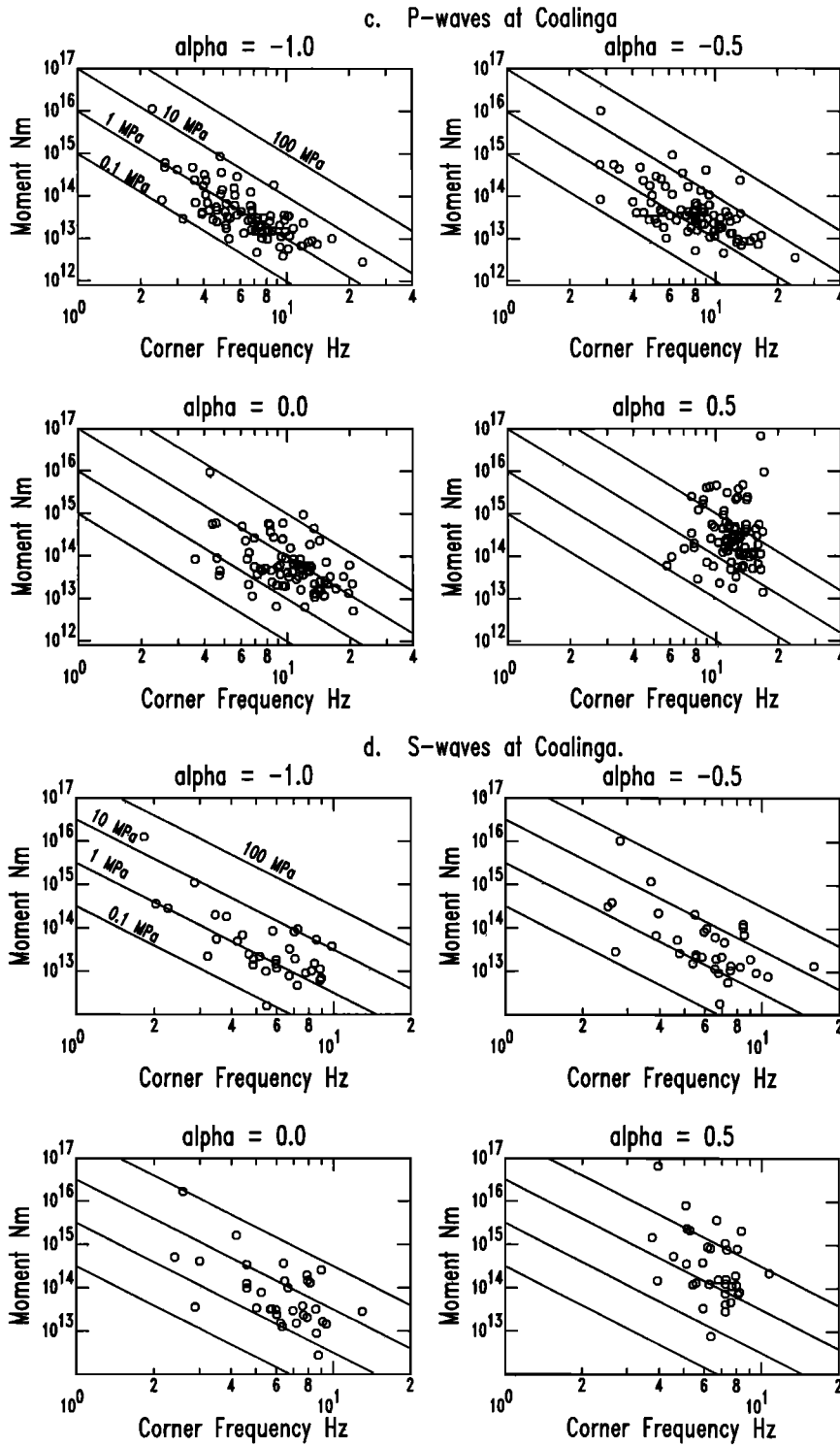


Fig. 10. (continued)

the t^* values measured by Frankel and Wennerberg are comparable to the t^* values determined at the Sierra Nevada sites in the present study. *Anderson and Hough* [1984] measured attenuation at several alluvium sites in California and found S wave t^* values that ranged from roughly 0.055 to 0.085 s. These values are slightly smaller but comparable to the t^* values determined for the alluvium sites near Coalinga. We conclude that the range of frequency-independent S wave t^* values for near-surface attenuation in California is about a factor of 10, ranging from roughly 0.01 to 0.10 s. Table 2

can be used as a starting point to estimate attenuation in the near surface from the site geology.

The source parameters determined in this study varied significantly depending on the region (Figure 10). Both seismic moments and stress drops were smaller at Loma Prieta than at Coalinga or Mammoth Lakes. The larger moments at Coalinga and Mammoth Lakes are not surprising, since both the Coalinga aftershock sequence and the earthquake sequence at Mammoth Lakes had unusually large magnitude earthquakes. The variation of average stress drop between the

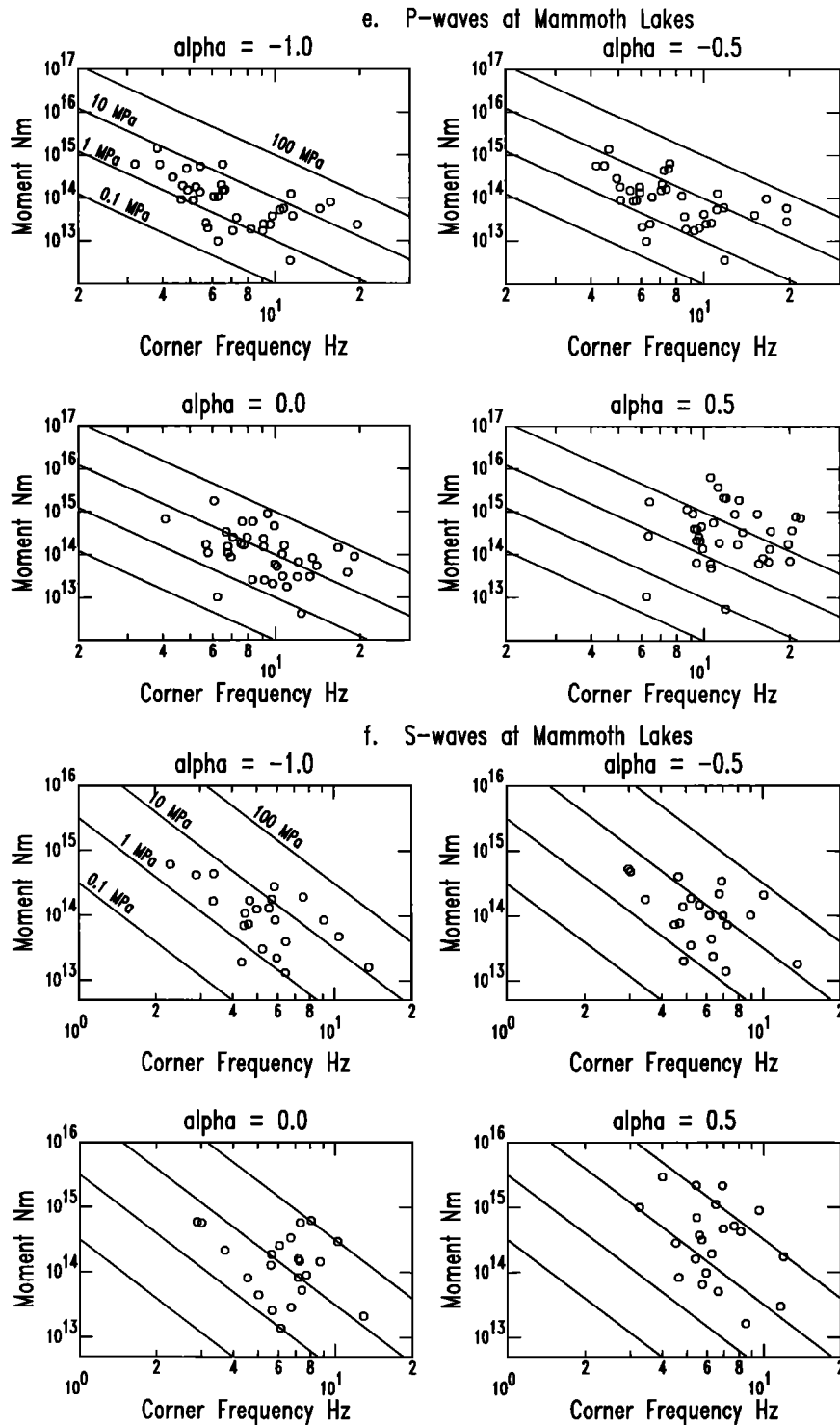


Fig. 10. (continued)

regions is more difficult to explain and is potentially very important. Stress drops at Loma Prieta were approximately a factor of 5 smaller than at Coalinga or Mammoth Lakes (Figure 10).

One possible explanation for the variation in stress drops is the different stress regimes in each region. Stress drops might be expected to be greatest in an area of thrust faulting [e.g., Sibson, 1974; McGarr, 1984] such as Coalinga. This would explain why the stress drops were greater at Coalinga than at Loma Prieta, but does not explain why stress drops are

nearly the same at Coalinga and Mammoth Lakes. Another factor that can affect stress drop is pore fluid pressure. A greater pore fluid pressure within the San Andreas Fault Zone has been proposed by Rice [1990] in order to explain the apparent weakness of the fault. A greater pore fluid pressure within the fault zone also allows faulting when the principal stress is nearly perpendicular to the fault as is observed along much of the San Andreas Fault [Zoback et al., 1987]. The lower stress drops at Loma Prieta could be an indication of high pore fluid pressure along the San Andreas Fault.

TABLE 4. Selected *P* Wave Source Parameters for Loma Prieta

Date	Time	Latitude N	Longitude W	No. of Fits	Seismic Moment $\times 10^{11}$ Nm	Corner Frequency Hz	Stress Drop MPa
October 25	13 00:41	36° 54.10'	121° 38.15'	6	2950 ⁺⁴⁷⁹ -412	3.6 ^{+0.4} -0.4	1.4 ^{+0.4} -0.3
October 22	9 44:58	36° 55.90'	121° 39.99'	9	610 ⁺⁹⁶ -83	10.8 ^{+2.6} -2.1	7.9 ^{+3.9} -2.6
November 3	10 47:56	36° 55.99'	121° 40.91'	11	332 ⁺¹³³ -95	11.9 ^{+1.9} -1.7	5.6 ^{+3.0} -2.0
October 30	6 31:27	36° 56.06'	121° 40.90'	18	157 ⁺²⁶ -22	5.4 ^{+0.7} -0.6	0.25 ^{+0.08} -0.06
October 31	18 12:01	37° 3.63'	121° 55.13'	11	94.3 ^{+17.1} -14.5	15.7 ^{+2.6} -2.2	3.7 ^{+2.0} -1.4
October 31	6 50:07	37° 8.42'	121° 58.96'	16	35.5 ^{+7.2} -6.0	14.1 ^{+1.9} -1.7	1.0 ^{+0.3} -0.3
October 30	12 58:36	37° 7.97'	121° 54.65'	18	25.0 ^{+4.1} -3.5	11.0 ^{+1.7} -1.5	0.34 ^{+0.11} -0.09
October 23	10 11:21	37° 8.35'	121° 59.35'	9	10.4 ^{+1.6} -1.4	27.6 ^{+3.1} -2.8	2.2 ^{+0.6} -0.5
October 25	13 31:35	37° 8.62'	121° 59.21'	8	6.3 ^{+1.7} -1.4	26.8 ^{+5.2} -4.4	1.2 ^{+0.6} -0.4
October 29	6 31:24	37° 8.43'	121° 54.89'	17	4.7 ^{+0.6} -0.6	20.1 ^{+3.0} -2.6	0.39 ^{+0.12} -0.09
October 22	3 26:57	37° 8.39'	122° 0.01'	9	2.4 ^{+0.3} -0.3	17.9 ^{+2.6} -2.2	0.14 ^{+0.04} -0.03

Source parameters are log averages calculated using $\alpha = -0.5$ fits. The earthquakes were selected to give a range of moments, corner frequencies, and stress drops. Errors are the standard deviation of the mean.

CONCLUSIONS

Least squares best fits have been calculated to 8200 Fourier spectra of earthquakes from Coalinga, Mammoth Lakes, and the Santa Cruz Mountains, California. The three source parameters in the model were the low-frequency spectral asymptote (Ω_0), corner frequency (f_c), and source spectral falloff (γ). Attenuation was determined by two parameters, t_0^* and α , via the equation $t^* = t_0^* f^{-\alpha}$. The results were as follows.

1. The best fitting Q decreased with increasing frequency for the high and moderate attenuation sites (α was negative). The parameter α was poorly resolved for the low attenuation sites. Negative values of α were also necessary in order that t_0^* did not vary systematically with the low-frequency spectral asymptote.

2. P and S wave attenuation as measured by t_0^* varied by up to a factor of 10, depending on site geology. On average, alluvium sites near Coalinga had the highest attenuation, while sites within the Sierra Nevada near Mammoth Lakes had the lowest attenuation. At Loma Prieta, the lowest attenuation occurred at sites located on Franciscan assemblage rocks, and the greatest attenuation occurred at the youngest age (Pliocene and Miocene) rock sites.

3. The relative amplification between sites varied in each of the three regions by approximately a factor of 5 and correlated with near-surface geology usually increasing with attenuation.

4. The average spectral falloff for P waves was close to $f^{-2.5}$ for the low attenuation sites in the Sierra Nevada. The

spectral falloff due to the source for P waves was therefore apparently limited to be no greater than $f^{-2.5}$.

5. Source parameters varied significantly depending on the value of α used in the spectral fits. Seismic moments trended approximately as f_c^{-3} only when the fits were calculated using negative values for α .

6. Seismic moments and stress drops varied depending on the region. Stress drops were smaller in the Santa Cruz Mountains compared to Coalinga or Mammoth Lakes by about a factor of 5. For α equal to -0.5 , stress drops ranged from approximately 0.05 to 8.0 MPa in the Santa Cruz Mountains and from approximately 0.2 to 50 MPa at Coalinga and Mammoth Lakes. Possible causes for the regional variation in stress drop include changes in the orientation of the principal stresses and variations of pore fluid pressure between the three areas.

There are several aspects of this study that can be pursued further. Frequency-dependent site amplifications such as resonances are certainly a source of error in the determination of the fit parameters, especially the corner frequency. Also, we cannot eliminate the possibility that frequency-dependent site amplifications biased the determination of the parameter α . Frequency-dependent site amplifications could be considered in a study of this type by jointly inverting the spectra in a manner similar to *Boatwright et al.* [1991] or *Scherbaum* [1990]. This type of global inversion was beyond the scope of the present paper.

The lower average stress drop and larger P to S wave corner frequency ratio at Loma Prieta compared to Mammoth Lakes or Coalinga also deserves further analysis. If these results can

be shown to represent genuine differences between regions, it would indicate fundamental differences in source properties of small earthquakes on a regional basis. It may also be possible to use the variation of stress drop between individual earthquakes within each region to examine the spatial variation of stress drop in the seismogenic zone.

Acknowledgments. Critical reviews were provided by John Boatwright, Arthur Frankel, and Raul Castro. The Seismic Analysis Code developed at Lawrence Livermore National Laboratory was used to make many of the plots. Map of the Loma Prieta region was provided by Jonathan Lees. This research was supported by the U. S. Geological Survey, Department of Interior, under award number 14-08-0001-G1857.

REFERENCES

- Aki, K., Scaling law of seismic spectrum, *J. Geophys. Res.*, **72**, 1217-1231, 1967
- Aki, K., Attenuation of shear-waves in the lithosphere for frequencies from 0.05 to 25 Hz, *Phys. Earth Planet. Inter.*, **21**, 50-60, 1980.
- Anderson, J. G., Implication of attenuation for studies of the earthquake source, in *Earthquake Source Mechanics*, *Geophys. Monogr. Ser.*, vol. 37, edited by S. Das, J. Boatwright, and C. H. Scholz, pp. 31-318, AGU, Washington, D. C., 1986.
- Anderson, J. G., and S. E. Hough, A model for the shape of the Fourier amplitude spectrum of acceleration at high frequencies, *Bull. Seismol. Soc. Am.*, **74**, 1969-1994, 1984.
- Andrews, D. J., Objective determination of source parameters and similarity of earthquakes of different size, in *Earthquake Source Mechanics*, *Geophys. Monogr. Ser.*, vol. 37, edited by S. Das, J. Boatwright, and C. H. Scholz, pp. 259-268, AGU, Washington, D. C., 1986.
- Archuleta, R. J., E. Cranswick, C. Mueller, and P. Spudich, Source parameters of the 1980 Mammoth Lakes, California, earthquake sequence, *J. Geophys. Res.*, **87**, 4595-4607, 1982.
- Bailey, R. A., Geologic map of Long Valley caldera, Mono-Inyo craters volcanic chain, and vicinity, Eastern California, U. S. Geol. Surv., Denver, Co., 1989.
- Blakeslee, S. M., and P. Malin, High-frequency site effects at two Parkfield downhole and surface stations, *Bull. Seismol. Soc. Am.*, **81**, 332-345, 1991.
- Boatwright, J., Detailed spectral analysis of two small New York State earthquakes, *Bull. Seismol. Soc. Am.*, **68**, 1117-1131, 1978.
- Boatwright, J., J. B. Fletcher, and T. E. Fumal, A general inversion scheme for source, site, and propagation characteristics using multiply recorded sets of moderate-sized earthquakes, *Bull. Seismol. Soc. Am.*, **81**, 1754-1782, 1991.
- Boore, D. M., and J. Boatwright, Average body-wave radiation coefficients, *Bull. Seismol. Soc. Am.*, **74**, 1615-1621, 1984.
- Borcherdt, R. D., J. B. Fletcher, E. G. Jensen, G. L. Maxwell, J. R. VanSchaack, R. E. Warrick, E. Cranswick, M. J. S. Johnston, and R. McClearn, A general earthquake-observation system (GEOS), *Bull. Seismol. Soc. Am.*, **75**, 1783-1825, 1985.
- Brabb, E. E., and T. W. Dibblee, Jr., Preliminary geologic map of the Castle Rock Ridge quadrangle, Santa Cruz and Santa Clara counties, California, *U.S. Geol. Surv. Open File Rep.*, 79-659, 1979.
- Brune, J. N., Tectonic stress and the spectra of seismic shear waves from earthquakes, *J. Geophys. Res.*, **75**, 4997-5009, 1970. (Correction, *J. Geophys. Res.*, **76**, 5002, 1971.)
- Caccci, M. S. and W. P. Cacheris, Fitting curves to data, *Byte Mag.*, 340-360, May, 1984.
- Castro, R. R., J. G. Anderson, and S. K. Singh, Site response, attenuation and source spectra of S waves along the Guerrero, Mexico subduction zone, *Bull. Seismol. Soc. Am.*, **80**, 1481-1503, 1990.
- Chouet, B. K., K. Aki, and M. Tsujiura, Regional variation of the scaling law of earthquake source spectra, *Bull. Seismol. Soc. Am.*, **68**, 49-79, 1978.
- Clark, J. C., Preliminary geologic and gravity maps of the Santa Cruz - San Juan Bautista area, Santa Cruz, Santa Clara, Monterey, and San Benito Counties, California, *U.S. Geol. Surv. Open File Map*, 70-82, 1970.
- Cranswick, E., R. Wetmiller, and J. Boatwright, High-frequency observations and source parameters of microearthquakes recorded at hard-rock sites, *Bull. Seismol. Soc. Am.*, **75**, 1535-1567, 1985.
- De Natale, G., R. Madariaga, R. Scarpa, and A. Zollo, Source parameter analysis from strong motion records of the Friuli, Italy, earthquake sequence (1976-1977), *Bull. Seismol. Soc. Am.*, **77**, 1127-1146, 1987.
- Dibblee, T. W., Jr., Geologic map of the Coalinga quadrangle, California, *U. S. Geol. Surv. Open File Rep.*, 71-87 4, 1971a.
- Dibblee, T. W., Jr., Geologic map of the Joaquin rocks quadrangle, California, *U. S. Geol. Surv. Open File Rep.*, 71-87 8, 1971b.
- Dibblee, T. W., Jr., and E. E. Brabb, Preliminary geologic map of the Los Gatos quadrangle, Santa Clara and Santa Cruz counties, California, *U. S. Geol. Surv. Open File Rep.*, 78-453, 1978.
- Dibblee, T. W., Jr. and E. E. Brabb, Preliminary geologic map of the Loma Prieta quadrangle, Santa Cruz and Santa Clara counties, California, *U. S. Geol. Surv. Open File Rep.*, 80-944, 1980.
- Dibblee, T. W., Jr., E. E. Brabb, and J. C. Clark, Preliminary geologic map of the Laurel quadrangle Santa Cruz and Santa Clara counties, California, *U. S. Geol. Surv. Open File Rep.*, 78-84, 1978.
- Dysart, P. S., J. A. Snoke, and I. S. Sacks, Source parameters and scaling relations for small earthquakes in the Matushiro region, southwest Honshu, Japan, *Bull. Seismol. Soc. Am.*, **78**, 571-589, 1988.
- Eberhart-Phillips, D., Active faulting and deformation of the Coalinga anticline as interpreted from three-dimensional velocity structure and seismicity, *J. Geophys. Res.*, **94**, 15,565-15,586, 1989.
- Fehler, M., Locations and spectral properties of earthquakes accompanying an eruption of Mount St. Helens, *J. Geophys. Res.*, **90**, 12,729-12,740, 1985.
- Fehler, M. and W. S. Phillips, Simultaneous inversion for Q-parameters and source parameters of microearthquakes accompanying hydraulic fracturing in granitic rock, *Bull. Seismol. Soc. Am.*, **81**, 553-575, 1991.
- Fletcher, J. B., Spectra from high-dynamic range digital recordings of Oroville, California aftershocks and their source parameters, *Bull. Seismol. Soc. Am.*, **70**, 735-756, 1980.
- Fletcher, J. B. and J. Boatwright, Source parameters of Loma Prieta aftershocks and wave propagation characteristics along the San Francisco Peninsula from a joint inversion of digital seismograms, *Bull. Seismol. Soc. Am.*, **81**, 1783-1812, 1991.
- Frankel, A., The effects of attenuation and site response on the spectra of microearthquakes in the northeastern Caribbean, *Bull. Seismol. Soc. Am.*, **72**, 1379-1402, 1982.
- Frankel, A., and L. Wennerberg, Microearthquake spectra from the Anza, California, seismic network: site response and source scaling, *Bull. Seismol. Soc. Am.*, **79**, 581-609, 1989.
- Hanks, T. C., b values and ω^{-2} seismic source models: Implications for tectonic stress variations along active crustal fault zones and the estimation of high-frequency strong ground motion, *J. Geophys. Res.*, **84**, 2235-2242, 1979.
- Hanks, T. C., f_{max} , *Bull. Seismol. Soc. Am.*, **72**, 1867-1879, 1982.
- Hough, S. E., J. G. Anderson, J. Brune, F. Vernon III, J. Berger, J. Fletcher, L. Haar, T. Hanks, and L. Baker, Attenuation near Anza, California, *Bull. Seismol. Soc. Am.*, **78**, 672-691, 1988.
- Hough, S. E., L. Seeber, A. Lerner-Lam, J. G. Armbruster, and H. Guo, Empirical Green's function analysis of Loma Prieta aftershocks, *Bull. Seismol. Soc. Am.*, **81**, 1737-1753, 1991.
- Ihaka, G. R., Ruaumoko, Ph.D dissertation, University of California, Berkeley, 1985.
- McGarr, A., Scaling of ground motion parameters, state of stress, and focal depth, *J. Geophys. Res.*, **89**, 6969-6979, 1984.
- McGarr, A., C. Mueller, J. B. Fletcher, and M. Andrews, Ground-motion and source parameters of the Coalinga earthquake sequence, in *The Coalinga, California, Earthquake of May 2, 1983, Prof. Pap. 1487*, edited by M. J. Rymer and W. L. Ellsworth, pp. 215-233, U. S. Geological Survey, Menlo Park, Ca., 1990.
- Mueller, C., P. Spudich, E. Cranswick, and R. Archuleta, Preliminary analysis of digital seismograms from the Mammoth Lakes, California earthquake sequence of May-June, 1980, *U. S. Geol. Surv. Open File Rep.*, 81-155, 1981.
- Mueller, C. S., E. Sembera, and L. Wennerberg, Digital recordings of aftershocks of the May, 2 1983 Coalinga, California earthquake, *U. S. Geol. Surv. Open File Rep.*, 84-697, 1984.

- Nelder, J. A. and R. Mead, A simplex method for function minimization, *Computer Journal*, 7, 308, 1965.
- Rice, J. R., Fault stress states, pore pressure distributions, and the weakness of the San Andreas Fault (abstract), *EOS Trans. AGU*, 71, 1652, 1990.
- Rovelli, A., O. Bonamassa, M. Cocco, M. Di Bona, and S. Mazza, Scaling laws and spectral parameters of the ground motion in active extensional areas in Italy, *Bull. Seismol. Soc. Am.*, 78, 530-560, 1988.
- Scherbaum, F., Combined inversion for the three-dimensional Q structure and source parameters using microearthquake spectra, *J. Geophys. Res.*, 95, 12423-12438, 1990.
- Shearer, P. M. and J. A. Orcutt, Surface and near-surface effects on seismic waves- theory and borehole seismometer results, *Bull. Seismol. Soc. Am.*, 77, 1168-1196, 1987.
- Sibson, R., Frictional constraints on thrust, wrench, and normal faults, *Nature*, 249, 542-544, 1974.
- Simpson, D., S. Hough, and A. Lerner-Lam, Earthquake response, *EOS Trans. AGU*, 70, 1450, 1989.
- Snoke, J. A., Stable determination of (Brune) stress drops, *Bull. Seismol. Soc. Am.*, 77, 530-538, 1987.
- Spudich, P., E. Cranswick, J. Fletcher, E. Harp, C. Mueller, R. Navarro, J. Sarmiento, J. Vinton, R. Warrick, Acquisition of digital seismograms during the Mammoth Lakes, California, earthquake sequence May-June 1980, *U. S. Geol. Surv. Open File Rep.*, 81-38, 1981.
- Trifunac, M. D., Stress estimates for the San Fernando, California, earthquake of February 9, 1971: Main event and 13 aftershocks, *Bull. Seismol. Soc. Am.*, 62, 721-750, 1972.
- Tucker, B. E., and J. N. Brune, S wave spectra and source parameters for aftershocks of the San Fernando earthquake of February 9, 1971, in *Geological and Geophysical Studies*, vol. 3, pp. 69-122, San Fernando Earthquake of February 9, 1971 National Oceanic and Atmospheric Administration, Washington, D. C., 69-122, 1973.
- Walck, M. C., Seismic attenuation models of Asian explosions recorded at NORESS, *Report SAND88-2155*, Sandia Natl. Lab., Albuquerque, N. M., 1988.
- Zoback, M. D., J. P. Eaton, J. H. Healy, L. Jones, V. S. Mount, D. Oppenheimer, C. B. Raleigh, P. Reasenber, O. Scotti, J. Suppe, C. Wentworth, I. G. Wong, and M. L. Zoback New evidence on the state of stress of the San Andreas Fault system, *Science*, 238, 1105-1111, 1987.

R. J. Archuleta and G. T. Lindley, Department of Geological Sciences and Institute for Crustal Studies, University of California, Santa Barbara, CA, 93106.

(Received February 8, 1991;
revised February 14, 1992;
accepted March 3, 1992.)